The formation and growth of a cross kink in a rope under torsion: An interpretation based on structural mechanics

Luca Lanzoni, Angelo Marcello Tarantino

PII: S0997-7538(22)00167-X
DOI: https://doi.org/10.1016/j.euromechsol.2022.104720
Reference: EJMSOL 104720

To appear in: *European Journal of Mechanics / A Solids*

Received date : 27 May 2022
Accepted date : 22 June 2022

Please cite this article as: L. Lanzoni and A.M. Tarantino, The formation and growth of a cross kink in a rope under torsion: An interpretation based on structural mechanics. *European Journal of Mechanics / A Solids* (2022), doi: https://doi.org/10.1016/j.euromechsol.2022.104720.

The formation and growth of a cross kink in a rope under torsion: An interpretation based on structural mechanics

Luca Lanzoni[1], Angelo Marcello Tarantino[2]

May 26, 2022

[1]DIEF, Università di Modena e Reggio Emilia, via P. Vivarelli 10, 41125, Modena, Italy, e-mail: luca.lanzoni@unimore.it,

[2]DIEF, Università di Modena e Reggio Emilia, via P. Vivarelli 10, 41125, Modena, Italy, e-mail: angelomarcello.tarantino@unimore.it

Abstract

The application of large twistings to a thin rope is known to cause the occurrence and evolution of an intermediate cross kink. Using classical linear elastic structural mechanics, the branched equilibrium path, which characterizes the kink formation, has been obtained. This path is characterized by increasing torsional stiffness. Some energy considerations have been formulated to motivate why the rope moves along the branched path generating the cross kink.

Keywords: Torsion; Rope; Equilibrium; Structural mechanics, Cross kink.

1 Introduction

The formation of kinks has been studied in many practical contexts. Rosenthal [1] considered marine cables as tension members, for which serious structural failures can occur as a result of the so-called hockling. This problem derives from the twisting moments that develop in a cable, making the applied tensions insufficient to keep the cable taut, thus causing the formation of a loop or hockle. Using the Greenhill's formula [2], Rosenthal [1] formulated a stability criterion on end twisting moments and final axial forces for preventing hockling in cables. Similar analyses in ocean engineering was performed for pipelines, electromechanical submarine cables, catenary risers and jacketed optical fibers (see Ross [3], Yabuta [4], Neto and de Arruda Martins [5]).

As shown by Goyal et al. [6], at small length scales, some striking similarities exist between the interwound DNA supercoils and the hockles of the marine

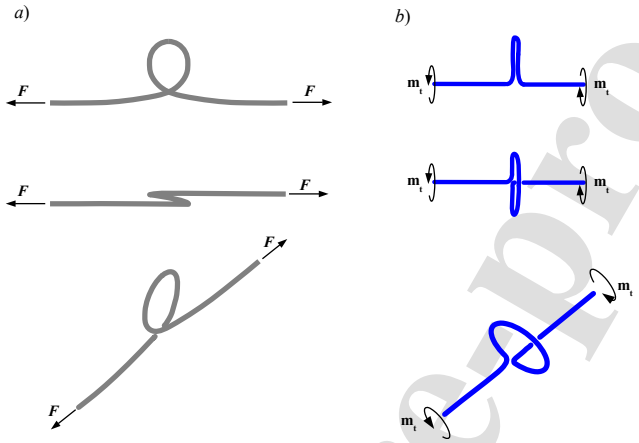

Figure 1: Two different types of kinks. a) The Coyne's model [9]. b) The model studied in this paper.

cables. In particular, the bending and torsional stiffness of DNA molecules greatly influences its functional behavior, including gene expression (see Mehta and Kahn [7], Smith at al. [8]).

For cables under tension and torsion, an important contribution was made by Coyne [9]. He, using the basic differential equations of the *Elastica*, computed in closed form the force versus displacement at the ends of a twisted cable and the point at which the cable flips into a loop. The model studied by Coyne is shown in Fig. 1a.

For the same problem, Thompson and Champneys [10] compared the periodic helical modes predicted by Greenhill [2] and Love [11] with the localized modes investigated by Coyne [9]. In detail, they show that for a long rod an unstable helix is initially the preferred energetically favorable mode of deformation. As the amplitude of the torsional rotation increases, the helix can progressively localize, continuously deforming until to form a single kink. On the basis of an experimental analysis, they also conjectured that most likely the equilibrium paths observed were not a strictly consequent to buckling modes, provided by a classic bifurcation and stability analysis, being these paths quite influenced by technical imperfections, such as an initial curvature of the cable.

In this paper, the cross kinks in a rope generated exclusively by torques applied to its ends are investigated. In this case, as shown in Fig. 1b, the kink has geometric characteristics different from those studied in the aforementioned papers, which refer to cables subjected mainly to axial tension force. In particular, the kink now occurs in a plane orthogonal to the axis of the rope. The succession of phases that contribute to the formation of a cross kink are described below.

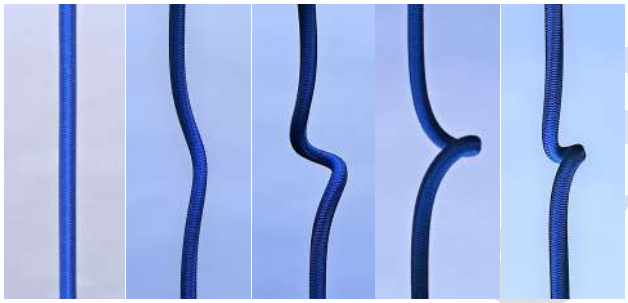

Figure 2: The formation of cross kink in a rope subjected to torque.

When a rope is twisted to a sufficiently large extent, a small lateral deviation, similar to two half waves, can be observed in its central part, while the lateral parts maintain their rectilinear shape. By increasing the external torque, this small initial ripple develops into a more showy structure similar to a single-pitch helix. This helix increases its radial extension while reducing the pitch until it turns into a horizontal ring. By further increasing the torque, the ring collapses on itself and then the process for the formation of a new cross kink is repeated and so on. For a real case, the phenomenon just described is shown in Fig. 2 through a succession of images.

For the previous problem, several times mentioned in the Literature (see for example the Introduction of the paper by Ciarletta and Destrade [12]) a mechanical model capable of describing the appearance, development and formation of a cross kink, is proposed. Unfortunately, the Coyne's analysis [9], based on the theory of the *Elastica,* can no longer be applied due to the absence of the axial force, since it is physically evident that a rope cannot be compressed. Furthermore, the stability analysis of Love [11] is not valid either, as the phenomenon considered is fundamentally localized and not diffused along the entire rope.

In order to generate the kink, the rope must have low flexural and torsional stiffnesses. Consequently, the rope experiences low stresses and, in turn, also the strains can be assumed small. This allows, as done in all the previously cited papers, to adopt a linear constitutive law. The displacements are large, however the equilibrium equations that we will write do not depend on the magnitude of the displacements. With these premises, the problem will be studied in the context of linear structural mechanics.

After undergoing a torsional screwing of a certain amount, in the central part of the rope, that is in the most deformable part, a misalignment between the torque vector and the vector of the torsional rotation can occur.[1] This little imperfection is responsible for the initial ripple and the emergence of a small bending moment. Subsequently, by increasing the external torque, this

[1]This is in accordance with what is conjectured in [10].

central part of the rope, involved in the formation of the cross kink, witnesses the gradual growth of the bending moment and the decrease of the internal torque. These aspects are highlighted in Section 2. The torsional stiffness of the rope during the evolution of the central helix is determined in Section 3 through the application of the minimum total potential energy principle. The equilibrium path followed by the rope during the formation of the cross kink is shown in Section 4, where some energy considerations are also carried out. The branch point of the straight equilibrium path is computed in Section 5, where some experimental evidences are shown. The conclusions, delivered in Section 6, close the paper.

2 Modeling based on structural mechanics

The rope is a structural element without axial compressive stiffness, and with low flexural and torsional stiffness. The ends of the rope are free to move longitudinally (cf. Fig. 1b). It is remarked that the ends of the rope are left free to slide axially and move closer to each other. Before the lateral deviation, the rope is subjected to two twisting moments m_t (or torques), of opposite sign, applied at both ends. As shown in Fig. 3a, in this first phase, the vectors of these moments are coaxial with the axis of the rope.[2] Let's consider now a portion of the rope in the branched configuration with the aim of evaluating internal actions. As is evident from Fig. 3b, the two twisting moments, m_t and m_t', are no longer coaxial and, in general, not even coplanar. In the generic cross section A-A, where the cut has been made, concentrated forces (normal and shear forces) cannot arise because otherwise the translational equilibrium would be impossible. Bending moments m_f must be applied to cross section A-A to restore the rotational equilibrium. Thus in the middle portion l' of the rope a part of the twisting moment is transformed into bending moment (cf. Fig. 5).

To evaluate the internal actions in the generic cross section A-A, a static equivalence of the moments around the three axes of a local reference system, identified by the three unit vectors $\mathbf{i}$, $\mathbf{j}$ and $\mathbf{k}$ and origin coinciding with the centroid of the cross section G, can be used. As shown by Fig. 4, the vector of the external moment $\mathbf{m}_t$ has been translated parallel to itself by applying it in G. The following scalar components can be evaluated:

$$\begin{array}{l} m_x = \mathbf{m}_t \cdot \mathbf{i} = m_t \cos\alpha_x \\ m_y = \mathbf{m}_t \cdot \mathbf{j} = m_t \cos\alpha_y \\ m_t' = \mathbf{m}_t \cdot \mathbf{k} = m_t \cos\alpha_z \end{array} , \tag{1}$$

where $m_t = \mid \mathbf{m}_t \mid$ and the other quantities are pointed out in Fig. 4. The m_x and m_y components can be assembled to obtain the modulus of the overall

[2] Twisting moments are indicated by vectors with two arrows.

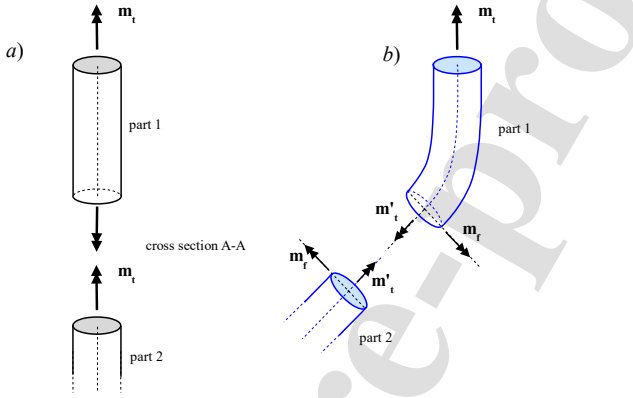

Figure 3: Internal actions in a generic cross section of the rope. a) Rectilinear equilibrium configuration. b) Branched equilibrium configuration.

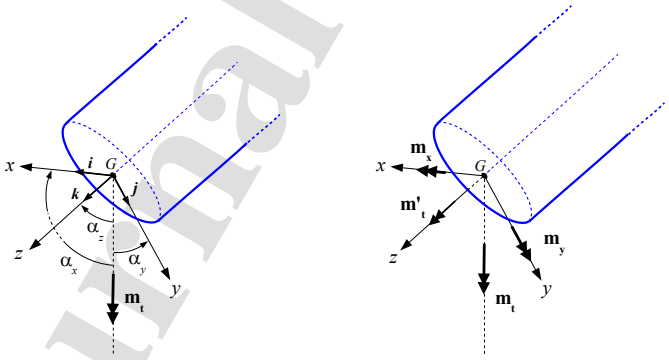

Figure 4: Twisting and bending moments in the cross section *A-A* of the branched configuration.

bending moment m_f acting on the cross section

$$m_f = \sqrt{m_x^2 + m_y^2} = m_t \sqrt{\cos^2 \alpha_x + \cos^2 \alpha_y} = m_t \sqrt{1 - \cos^2 \alpha_z} = m_t \sin \alpha_z. \tag{2}$$

In the previous equation the orthonormality condition of the direction cosines has been used.

In the following we will focus on the three moments m_t, m_t' and m_f. The equilibrium of one of the two parts of the rope illustrated in Fig. 3b leads to the following relationship between the three moments:

$$m_t^2 = (m_t')^2 + m_f^2. \tag{3}$$

The modulus of the external torque m_t is an input data of the problem and it must be considered as a variable function with a known law. The vector $\mathbf{m}_t$ can change its modulus, but not its direction. Moments m_t' and m_f are internal actions. The torque m_t' is measured along the tangent to the rope axis, orthogonally to the cross section. The bending moment m_f is evaluated orthogonally to the rope axis, in the plane of the cross section.

During the formation of the inner helix the three moments m_t, m_t' and m_f vary. The external torque m_t grows. For $\alpha_z = 0$ ($\alpha_x = \alpha_y = \frac{\pi}{2}$) the rope is in the initial rectilinear configuration, $m_t = m_t'$, and $m_f = 0$. As α_z grows, m_t' decreases and m_f arises. The bending moment m_f grows up to a maximum value for which a horizontal ring is formed. In this case, $\alpha_z = \frac{\pi}{2}$ ($\alpha_x = \alpha_y = 0$), $m_t' = 0$, and $m_t = m_f$.

Since the shear forces are zero, the bending moment is constant in modulus along the central portion l', except small connecting portions with the vertical axis. These curvilinear connections are modeled as cusps in order to have constant internal moments for them too. The evolution of the bending moment vector is described in Fig. 5. At the beginning, due to a small perturbation, a small bending moment is created almost orthogonal to the vertical axis of the rope. Increasing $\mathbf{m}_t$, the central portion l' assumes a configuration more and more distant from the rectilinear one. The bending moment vector grows remaining always orthogonal to the curved axis of the rope. In this phase, it changes modulus and direction with continuity. When the horizontal ring is formed, the bending moment vector is parallel to the vertical axis of the rope and it perfectly balances the external torque $\mathbf{m}_t$. As the bending moment increases, the torque in the branched portion of the rope decreases until it is completely canceled out when the horizontal ring is formed. The horizontal ring acts like a bending spring for the rope. Further increasing $\mathbf{m}_t$, the ring collapses on itself and then a second spiral forms and so on. In the following we will consider only the formation of the first cross kink.

Let's now analyze the kinematic parameters of the model. The θ angle indicates the overall torsional rotation of the rope. Given the linearity of the constitutive law we can write: $m_t = k_t \theta$. Before the formation of the intermediate spiral, the torsional stiffness for the straight rope is $k_t = \frac{G J_P}{l}$, where l is the length of the rope, G the modulus of tangential elasticity and J_P the

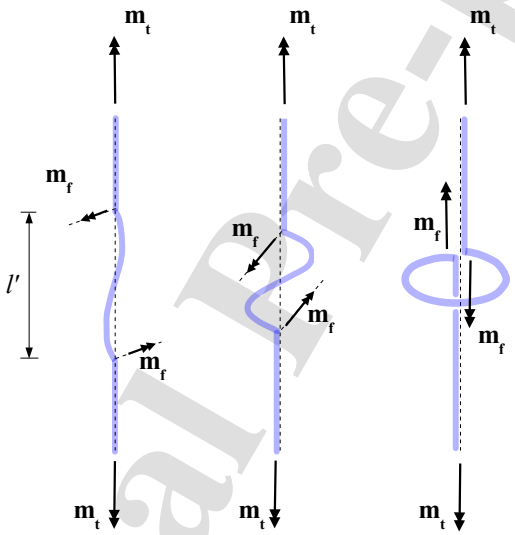

Figure 5: Evolution of the bending moment vector during the formation of the internal helix.

polar moment of inertia. For the circular cross section: $J_P = \frac{\pi R^4}{2}$, where R is the radius of the cross section. During the formation of the spiral, the torsional stiffness of the rope varies as a function of the α_z angle, $k_t = \hat{k}_t(\alpha_z)$. The θ' angle denotes the torsion angle of the only intermediate portion l'. θ' starts from the initial value θ_i, which characterizes the incipient formation of the spiral, and it gradually reduces to zero when the horizontal ring is generated for $\theta = \theta_f$. The flexion angle produced by the bending moment is indicated with the symbol ϕ. For the flexion of the central portion of the rope the following constitutive relationship holds: $m_f = k_f\,\phi$. The bending stiffness is $k_f = \frac{E\,J_x}{l'}$, where E is Young's modulus and J_x the moment of inertia. Given the axial symmetry of the cross section, $J_x = \frac{\pi R^4}{4}$ for any inclination in the plane of the bending moment. The α_z angle, formed by the axis of the rope with respect to the vertical axis (cf. Fig. 4), is the kinematic parameter that governs the evolution of the cross kink. For $\alpha_z = 0$ the rope is straight ($\theta < \theta_i$). By increasing α_z, the rope takes on a branched configuration ($\theta_i \leq \theta \leq \theta_f$). For $\alpha_z = \frac{\pi}{2}$ the horizontal ring is formed ($\theta = \theta_f$).

Once introduced the mechanical model and defined the notation, in the next Section, the torsional stiffness of the rope during the evolution of the cross kink is evaluated.

3 Application of the minimum total potential energy principle

The total potential energy Φ is defined as the strain internal energy minus the mechanical work done by the external loads. The first variation of functional Φ set equal to zero, $\delta\Phi = 0$, constitutes an alternative formulation of the equilibrium. The stability of a stationary point of Φ can be assessed by observing the sign assumed by the second variation of Φ at that point. The structural system is in fact in a stable equilibrium state if the value of the total potential energy Φ is a local minimum, $\delta^2\Phi > 0$.

In each single phase of the spiral formation, the torsional rotation balance for the rope can be expressed in the following classic form: $m_t = k_t(\alpha_z)\,\theta$. In order to evaluate the torsional stiffness $k_t(\alpha_z)$ as the α_z angle varies, $\alpha_z \in \left[0,\, \frac{\pi}{2}\right]$, the principle of minimum total potential energy will be applied in the following. The total potential energy is

$$\Phi(\theta) = \int_V \varphi(\theta)\, dv - m_t\,\theta, \tag{4}$$

where $\varphi(\theta)$ is the stored energy function and its integral in the volume V of the rope represents the strain internal energy. This integral can be split into two terms

$$\int_V \varphi(\theta)\, dv = (l - l') \int_A \varphi_1(\theta)\, da \,+ l' \int_A \varphi_2(\theta)\, da, \tag{5}$$

of which the first term relates to the two external portions of the rope with lengths $(l-l')/2$, while the second term concerns the central portion of the rope with length l', which experiences the evolution of the helix. Since the functions φ_1 and φ_2 do not depend on the variable z, the volume integrals have been reduced to surface integrals on area A of the cross section. These two integrals of the right side of (5) can be expressed as follows:

$$(l-l')\int_A \varphi_1(\theta)\,da = \frac{1}{2}\,\frac{(l-l')}{GJ_P}\,m_t^2 = \frac{1}{2}\,\frac{(l-l')}{GJ_P}\,k_t^2(\alpha_z)\,\theta^2, \tag{6}$$

$$l'\int_A \varphi_2(\theta)\,da = \frac{1}{2}\,\frac{l'}{GJ_P}\,(m_t')^2 + \frac{1}{2}\,\frac{l'}{EJ_x}\,m_f^2 =$$

$$\frac{1}{2}\,\frac{l'}{GJ_P}\,k_t^2(\alpha_z)\,\theta^2\cos^2\alpha_z + \frac{1}{2}\,\frac{l'}{EJ_x}\,k_t^2(\alpha_z)\,\theta^2\sin^2\alpha_z.$$

Equations $(1)_3$ and (2) have been used to obtain this latter expression. With (5) and (6), the condition of vanishing of the first variation of functional Φ gives

$$\left[\frac{(l-l')}{GJ_P} + \frac{l'}{GJ_P}\,\cos^2\alpha_z + \frac{l'}{EJ_x}\,\sin^2\alpha_z\right]k_t^2(\alpha_z)\,\theta - m_t = 0. \tag{7}$$

By comparing this equation with the elastic solution, $m_t = k_t(\alpha_z)\,\theta$, the expression of the torsional stiffness turns out to be

$$k_t(\alpha_z) = \frac{1}{\frac{(l-l')}{GJ_P} + \frac{l'}{GJ_P}\,\cos^2\alpha_z + \frac{l'}{EJ_x}\,\sin^2\alpha_z}. \tag{8}$$

The overall stiffness of the rope therefore takes the form of an elastic system consisting of springs connected in series.

Formula (8) shows the torsional stiffness that the rope exhibits during the creation of the cross kink. Let us consider the extreme values of this transformation. For $\alpha_z = 0$,

$$k_t(0) = \frac{1}{\frac{(l-l')}{GJ_P} + \frac{l'}{GJ_P}} = \frac{GJ_P}{l}, \tag{9}$$

that is, the stiffness of a perfectly vertical rope. For $\alpha_z = \frac{\pi}{2}$,

$$k_t\left(\frac{\pi}{2}\right) = \frac{1}{\frac{(l-l')}{GJ_P} + \frac{l'}{EJ_x}}, \tag{10}$$

that is, the terminal stiffness of the rope when the formation of the cross kink is over. In this case, the simple one-pitch helix is collapsed in a horizontal ring, and the flexion stiffness of this ring, rotated and placed orthogonally to the vertical axis of the rope, is completely converted into torsional stiffness.

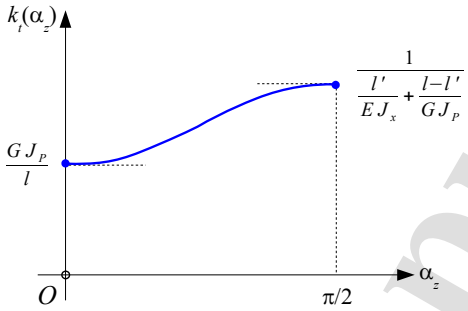

Figure 6: Graph of the torsional stiffness $k_t(\alpha_z)$.

The derivative of (8) is

$$\frac{dk_t(\alpha_z)}{d\alpha_z} = 2\left[\frac{l'}{GJ_P} - \frac{l'}{EJ_x}\right]\sin\alpha_z\cos\alpha_z\, k_t^2(\alpha_z). \tag{11}$$

It is always positive, namely the torsional stiffness of the rope grows during the formation of the spiral. This except at the end points, $\alpha_z = 0, \frac{\pi}{2}$, where the derivative vanishes. The fact that the derivative is null at the beginning of the process can be interpreted as the circumstance that the rope does not oppose the lateral deviation. The graph of the function $k_t(\alpha_z)$ is shown in Fig. 6.

The second variation of the total potential energy is

$$\delta^2\Phi(\theta) = \delta\left\{k_t(\alpha_z)\,\theta - m_t\right\} = k_t(\alpha_z), \tag{12}$$

and being $k_t(\alpha_z) > 0$, for any $\alpha_z \in \left[0, \frac{\pi}{2}\right]$, this means that all equilibrium solutions leading to cross kink are stable.

4 Equilibrium path and energy considerations

The equilibrium path, namely all the pairs (m_t, θ) that characterize the creation of the cross kink, are shown in Fig. 7. In the same plot, the linear elastic solution of the rope which preserves the rectilinear configuration is pointed out. The two lines are superimposed for an initial part. At the branch point θ_i, they, in addition to the same value, have also the same tangent, equal to $k_t(0) = \frac{GJ_P}{l}$. Then, by increasing θ, the branched path has higher torsional stiffnesses and therefore its equilibrium points show higher ordinates. Likewise, by fixing the external torque m_t, the equilibrium solutions of the branched path occur for smaller θ angles.

This last observation has energetic implications. A branched path solution exhibits both strain internal energy and potential energy of external loads less than the corresponding energies of the not branched solution. Namely, for any

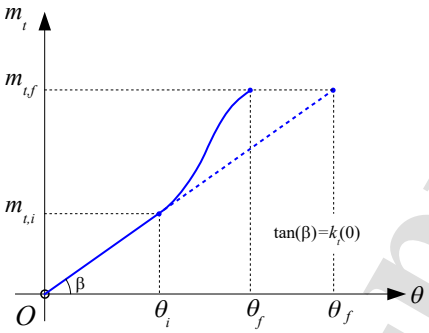

Figure 7: Equilibrium paths.

intermediate value of the external torque $m_t = k_t(\alpha_z)\,\theta = k_t(0)\,\bar{\theta}$ the following inequalities hold for the strain internal energy and potential energy of external loads:

$$\frac{1}{2}k_t(0)\,\theta_i^2 + \int_{\theta_i}^{\theta} k_t(\alpha_z)\,\theta\,d\theta < \frac{1}{2}k_t(0)\,\bar{\theta}^2, \qquad (13)$$

$$m_t\,\theta < m_t\,\bar{\theta},$$

where $m_t \in (m_{t,i},\, m_{t,f}]$ and $\bar{\theta} = m_t/k_t(0)$ is the torsional rotation of the not branched solution. Graphically this can also be seen from Fig. 7, where in particular the strain internal energy is the area subtended by the curves. This result allows us to make the following observation. The structural system, realized by the vertical rope, prefers to modify its geometry when it arrives at the branching point, starting the creation of a cross kink, because by following the consequent branched path it will have the possibility of storing a smaller amount of energy. This concept can also be applied later on during the intermediate stages of cross kink creation. That is, the system prefers to monotonically increase its torsional stiffness because this is energetically favorable for it.

The difference between the first members of the inequalities (13) represents the total potential energy studied in the previous Section. This potential is of the single-well type and it admits a unique stable solution for each value of the α_z angle. Indeed, by imposing the condition $\delta\Phi = 0$, for $\alpha_z = 0$, the equilibrium solution of the perfectly rectilinear rope is obtained; for α_z increasing from zero to $\frac{\pi}{2}$, all the progressive solutions that characterize the formation process of the central helix are evaluated and finally, for $\alpha_z = \frac{\pi}{2}$, the solution of the cross kink is computed.

Due to a small initial imperfection, the system abandons the rectilinear configuration and embarks on a branched path, characterized by growing torsional stiffness, which will end with the creation of the cross kink, through a succession

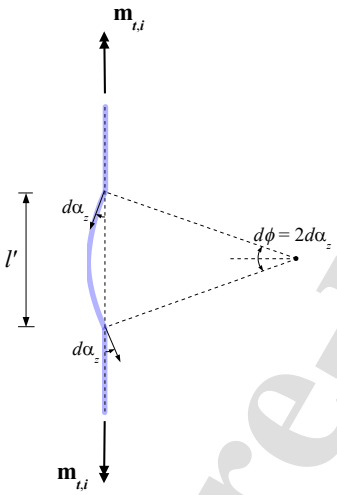

Figure 8: Small initial flexural perturbation.

of stable solutions. It does not exist therefore a classic bifurcation point (where $\delta^2\Phi = 0$), which is lost in an elastic system with geometric imperfections, but rather a branch point of the initial equilibrium path (where $\delta^2\Phi > 0$), that will be evaluated in the next Section.

5 The branch point and some experimental evidences

Let us consider the case in which the rope has already been subjected to an initial torsional screwing equal to θ_i. Now let's assume that, starting from this rectilinear configuration of the rope, a slight misalignment of the torque vector with the corresponding rotation vector occurs in the central part of the rope, where it is more flexible. This causes the emergence of a small bending moment dm_f which generates a slight curvature of the central portion of length l'. The situation described above is illustrated in Fig. 8.

These small second-order effects produce the following variations in the strain internal energy dW and in the mechanical work of the external loads dL ($d\phi = 2d\alpha_z$):

$$dW = \frac{1}{2}k_f(d\phi)^2 = 2k_f(d\alpha_z)^2, \quad dL = m_f\, d\phi = 2\, m_t(d\alpha_z)\sin d\alpha_z. \tag{14}$$

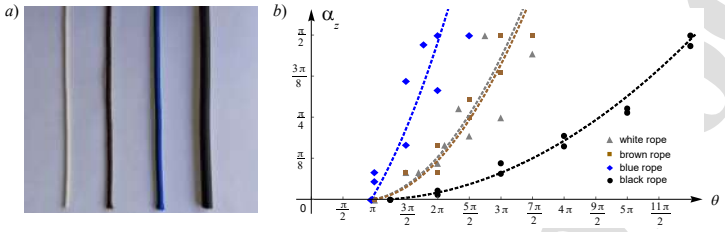

Figure 9: Experimental laws $\alpha_z = \hat{\alpha}_z(\theta)$. a) Types of rope used in the experimental tests. b) Experimental curves of α_z versus θ.

With these small energies, the energy balance can be imposed in the usual form

$$dW - \lambda\, dL = 0, \tag{15}$$

where the multiplier of the external loads λ is immediately set equal to one because we are interested in the minimum value of the external torque $m_{t,i} = k_t(0)\,\theta_i = \frac{GJ_P}{l}\,\theta_i$. By introducing expressions (14) into (15), the initial angle θ_i corresponding to the formation the cross kink is obtained

$$\theta_i = \frac{l}{l'}\,(1+\nu)\,. \tag{16}$$

To derive this formula the following relations have been used: $\sin d\alpha_z \simeq d\alpha_z$, $J_P = 2J_x$ and $E = 2G\,(1+\nu)$, where ν denotes the Poisson ratio. The pair $(m_{t,i},\, \theta_i)$ characterizes the beginning of the branched equilibrium path as shown in Fig. 7. Then, as described by Fig. 2, the process of forming the central helix develops by necessarily increasing the external torque.

At the end of the process, when the horizontal ring is formed, the internal bending moment balances the external torque $m_{t,f}$. In this condition the following relation can be written:[3]

$$l' = 2\pi\,\frac{EJ_x}{m_{t,f}}, \tag{17}$$

which can be used to determine the length l' once the torque $m_{t,f}$ is known, for example, through an experimental test.

For a specific rope, with assigned geometric and mechanical properties, experimental tests can be carried out in order to reproduce the constitutive curve shown in Fig. 7. In these types of tests, the main difficulty may lie in associating the values of the internal variable α_z with the overall angle of torsional rotation θ. For four different types of rope, in Fig. 9 the experimental laws $\alpha_z = \hat{\alpha}_z(\theta)$ are shown.

[3] In the case of low bending stiffnesses, the results of the linear theory retain a certain validity even in the case of large rotations (see [13], [14] and [15]).

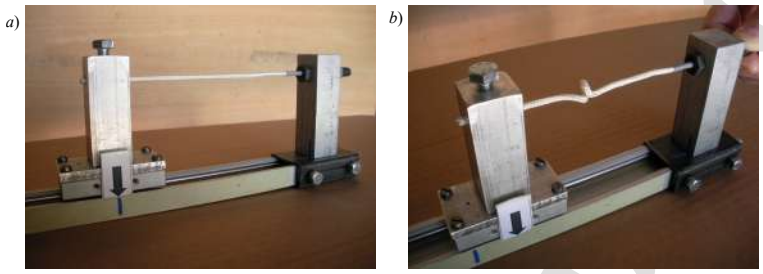

Figure 10: Experimental setup. a) Initial configuration. b) Deformed configuration.

The mechanical device used to obtain the experimental results (reported below in Fig. 9) is a very simple disposal composed by a horizontal guide and a pair of metallic supports for the rope. One of them (that on the right in Fig. 10) is fixed on the guide, the other one (that on the left in Fig. 10) is a slider which is free to move along the guide. As shown in the picture, one end of the rope is blocked to the slider support through a vertical bolt, whereas the other end is glued to the head of a horizontal screw which can rotate around its axis, that coincides with the longitudinal axis of the rope. Indeed, the points at which the rope is connected at the supports are perfectly aligned with each other. This allows imparting manually a torsional rotation by simply acting on the screw itself. An arrow has been marked on the slider, in such a way to highlight the horizontal displacement of the slider toward the fixed support as the imparted torsion increases. In this way, a large angle of twist can be imparted to the rope avoiding the occurrence of axial forces, thus reproducing the basic assumptions of the theoretical formulation.

Starting from the left, the first rope in Fig. 9a is made of nylon and has a diameter/length ratio (aspect ratio) equal to 3/100 (lengths are expressed in millimeters), the second is a synthetic rope with interwoven fibers and has an aspect ratio equal to 4/100, the third is a rope formed by many elastic threads held together by an external membrane in synthetic material and has an aspect ratio equal to 5/140, the fourth is a thin bar with circular cross section made of neoprene and has an aspect ratio equal to 10/350. For each of these four ropes, Fig. 9b shows the α_z values measured as the overall torsional rotation θ varies. Starting from the left, the first curve in Fig. 9b, which interpolates the experimental data, relates to the third rope, the second curve to the first rope, the third to the second rope and the fourth curve to the fourth rope. That is, among the four ropes, the third is the one that shows the least torsional stiffness and is the first to reach the formation of the horizontal ring for $\alpha_z = \frac{\pi}{2}$. An almost equal ratio l'/l have been measured for the first three ropes, while the fourth shows a higher values: The first has $l'/l = 0.28$, the second $l'/l = 0.32$, the third $l'/l = 0.3$ and the fourth $l'/l = 0.38$. It follows that the first three

ropes show a comparable initial branch angle θ_i, equal to or slightly higher than π, while the fourth rope shows a higher θ_i around $\frac{5}{4}\pi$.

6 Conclusions

Using linear elastic structural mechanics, the evolution of a central spiral, leading to the formation of a cross kink in a rope subjected to torque, has been modeled.

An initial imperfection is attributable to a slight loss of coaxiality between the torque vector and the corresponding rotation vector. It produces a small bending moment ensues. By increasing the external torque, this small initial imperfection evolves into a single-pitch helix. This central helix gradually reduces its pitch until it collapses into a horizontal ring. It is remarked that, unlike the classic bifurcation problems, there is a threshold for the external torque for which the branched solution takes place even if the unbranched path remains stable. In particular, critical points in the equilibrium paths disappear due to the presence of the imperfection, which guides the phenomenon. The equilibrium of a generic cross section of the branched configuration made it possible to evaluate the internal actions during the formation of the cross kink. The bending moment gradually increases until the horizontal ring is formed, where it completely balances the external torque. Vice versa, the internal torque decreases until it is completely canceled out in correspondence with the horizontal ring.

The torsional stiffness of the rope in each phase of the formation of the cross kink has been evaluated by applying the minimum total potential energy principle. It is an increasing monotonic function. Subsequently, the branched equilibrium path, that characterizes the evolution of the helix, has been obtained. This path is made up of all stable solutions and does not contain bifurcation points. It has also been highlighted that the rope prefers leave the straight path to follow the branched path since this involves lower energies. Through a balance of the second-order energies due to the initial small perturbation, the overall torsional rotation, for which the helix formation process begins, has been evaluated.

Finally, a criterion has been established for determining the length of the central portion of the rope which is involved in the formation of the cross kink. For four different types of thin ropes, some experimental evidences, based on the proposed structural modeling, has been shown.

Acknowledgment

Financial support from the Italian Ministry of Education, University and Research (MIUR) in the framework of the Project FISR 2019: "Eco Earth" (code 00245) is gratefully acknowledged.

References

[1] F. Rosenthal, The application of Greenhill's formula to cable hockling. *ASME J. Appl Mech.* **43** (1976) 681-683.

[2] A.G. Greenhill, On the strenght of shafting when exposed both to torsion and to end thrust. *Proc. Inst. of Mech. Engrs.* **34** (1883) 182-225.

[3] A.L. Ross, Cable kinking analysis and prevention. *ASME J. of Eng. for Industry* **99** (1977) 112-115.

[4] T. Yabuta, Submarine cable kink analysis. *Bull JSME* **27** (1984) 1821–1828.

[5] A.G. Neto, C. de Arruda Martins, Structural stability of flexible lines in catenary configuration under torsion. *Marine Structures* **34** (2013) 16-40.

[6] S. Goyal, N.C. Perkins, C.L. Lee, Torsional buckling and writhing dynamics of elastic cables and DNA, in Proceedings of ASME 2003: Design Engineering and Technical Conference, Chicago, USA, September 2–6, 2003, paper no. DETC2003/ MECH-48322.

[7] R.A. Mehta, J.D. Kahn, Designed hyperstable lac repressor DNA loop topologies suggest alternative loop geometries. *J. Mol. Biol.* **294** (1999) 67-77.

[8] S.B. Smith, Y.J. Cui, C. Bustamante, Overstretching B-DNA: the elastic response of individual double-stranded and single- stranded DNA molecules, *Science* **271** (1996) 795-799.

[9] J. Coyne, Analysis of the formation and elimination of loops in twisted cable. *J. Oceanic Eng.* **15** (1990)72–83.

[10] J.M.T. Thompson, A.R. Champneys, From helix to localized writhing in the torsional post-buckling of elastic rods, *Proc. of Roy. Soc. of London Serie*s A **452** (1996) 117–138.

[11] A.E.H. Love, *A treatise on the mathematical theory of elasticity*, 4th edn. Cambridge, UK: Cambridge University Press (1927).

[12] P. Ciarletta, M. Destrade, Torsion instability of soft solid cylinders. *IMA J. of Appl. Math.* **79** (2014) 804-819.

[13] L. Lanzoni, A.M. Tarantino, Finite anticlastic bending of hyperelastic solids and beams. *J. Elasticity* **131** (2018) 137-170, doi.org/10.1007/s10659-017-9649-y.

[14] L. Lanzoni. A.M. Tarantino. The bending of beams in finite elasticity. *J. Elasticity* **139** (2020) 91-121, doi.org/10.1007/s10659-019-09746-8.

[15] L. Lanzoni. A.M. Tarantino. Mechanics of High-Flexible Beams under Live Loads. *J. Elasticity* **140** (2020) 95-120, doi.org/10.1007/s10659-019-09759-3.

Author Agreement Statement

We the undersigned declare that this manuscript is original, has not been published before and is not currently being considered for publication elsewhere. We confirm that the manuscript has been read and approved by all named authors and that there are no other persons who satisfied the criteria for authorship but are not listed. We further confirm that the order of authors listed in the manuscript has been approved by all of us. We understand that the Corresponding Author is the sole contact for the Editorial process. He is responsible for communicating with the other authors about progress, submissions of revisions and final approval of proofs Signed by all authors as follows:

Luca Lanzoni 

Angelo Marcello Tarantino 

CONFLICT OF INTEREST

The authors declare that the present work has been realized in compliance with the Ethical Standards.

This study was funded by the aforementioned grant only.

Conflict of Interest: The authors declare that they have no conflict of interest.